SUPPORTING INFORMATION FOR

Coupling Strategies to Enhance Single-Molecule Magnet Properties of Erbium-Cyclooctatetraenyl Complexes

Jennifer J. Le Roy,[†] Liviu Ungur,[‡] Ilia Korobkov,[†] Liviu F. Chibotaru[‡] and Muralee Murugesu[†,*]

[†]Department of Chemistry, University of Ottawa, 10 Marie Curie, Ottawa, ON, K1N 6N5,. Canada

[‡]Theory of Nanomaterials Group and INPAC Institute for Nanoscale Physics and Chemistry, Katholieke Universiteit Leuven, Celestijnenlaan, 200F, 3001, Belgium.

Contents:

1. Single Crystal X-ray crystallography data

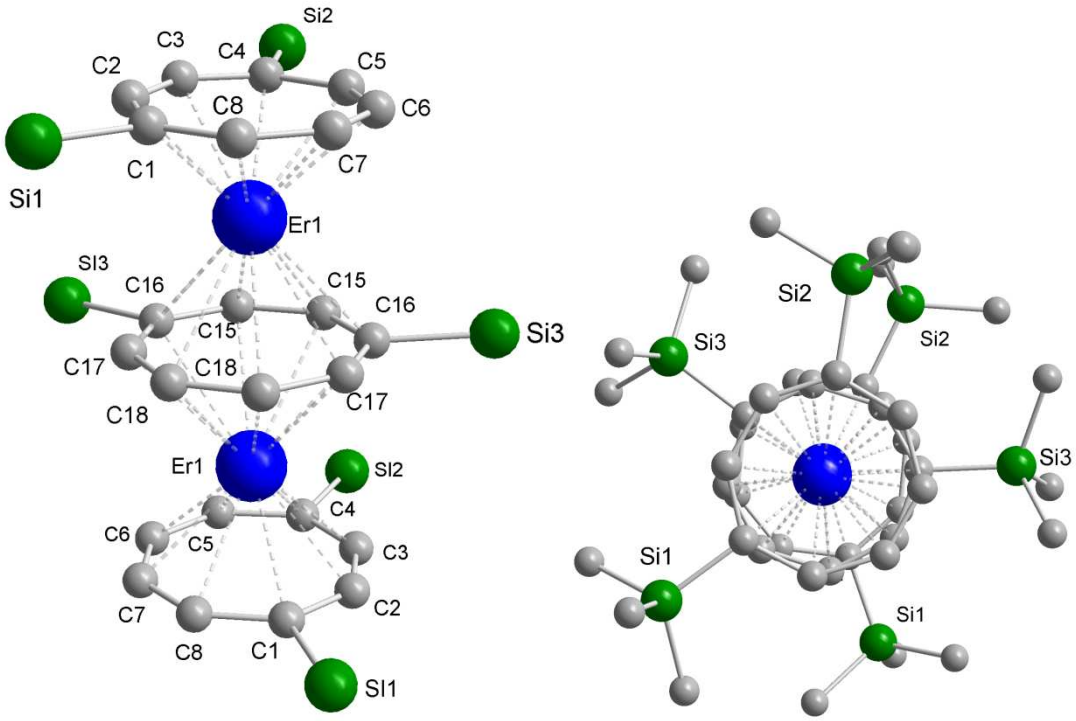

Figure S1. (left) Fully labelled molecular X-ray structure of **1**, H atoms and methyl substituents are omitted for clarity. (Right) Top view of **1**, H atoms are omitted for clarity, carbon atoms in all three layers are in a staggered arrangement. Colour code: blue (Er^{III}), green (Si), grey (C).

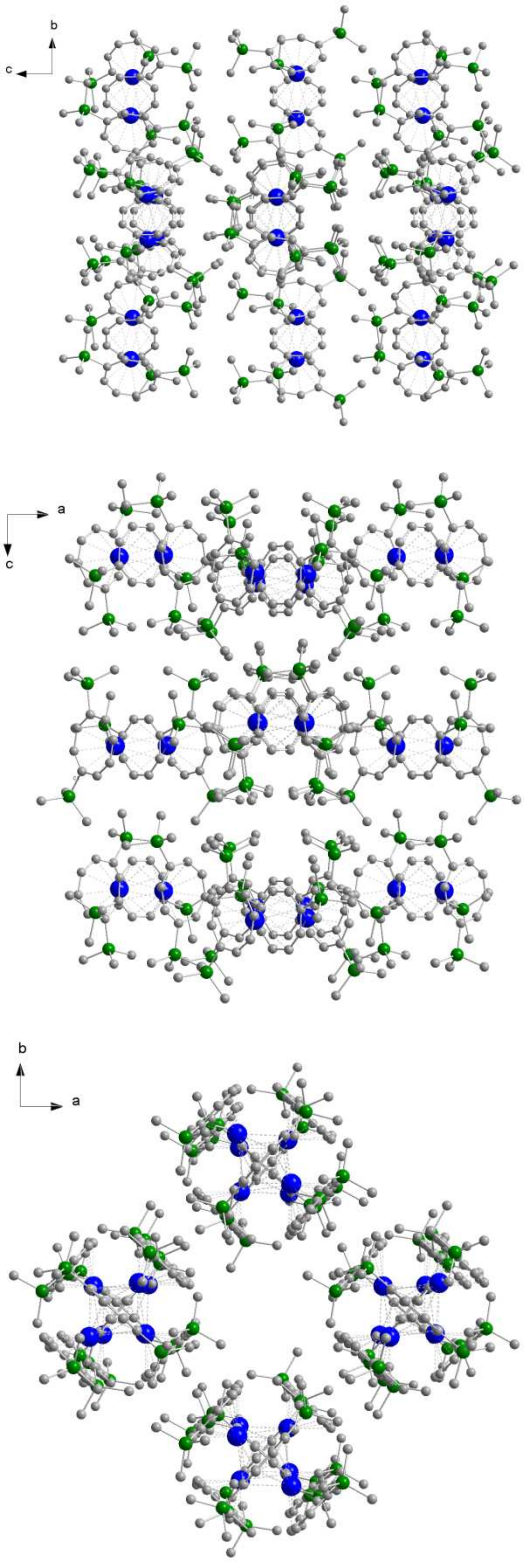

Figure S2. Packing arrangement of **1** looking down the *a* (top), *b* (center) and *c* (bottom) axis. H atoms are omitted for clarity. Color code: blue (Er^{III}), green (Si), grey (C).

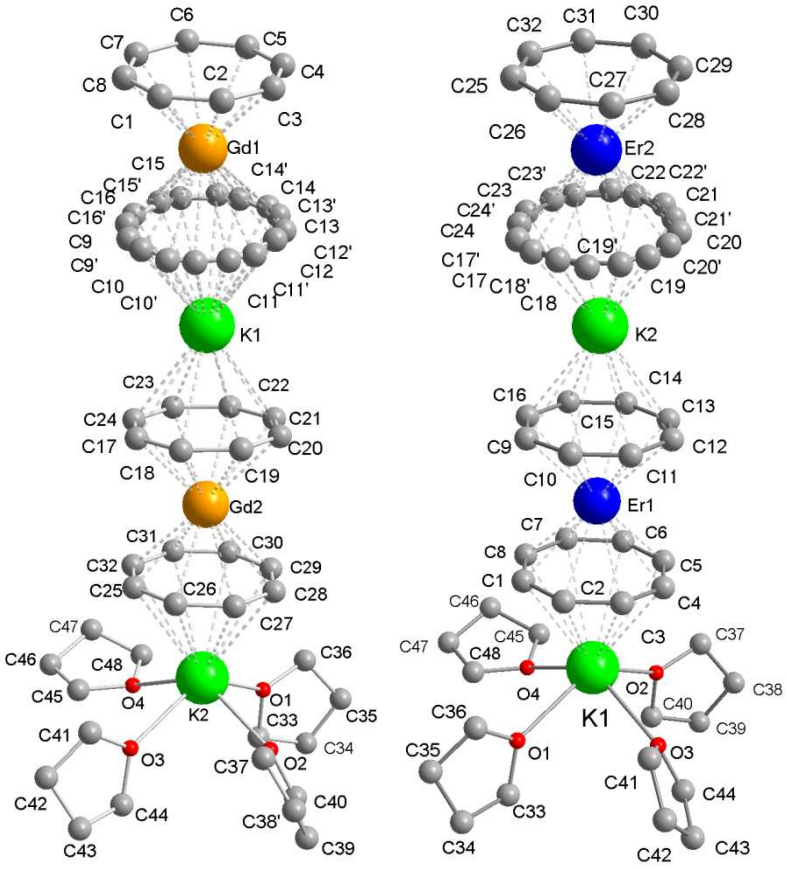

Figure S3. Fully labelled molecular X-ray structure of **2** (left) and **3** (right), H atoms are omitted for clarity. Colour code: Blue (Er^{III}), Orange (Gd^{III}), light green (K), grey (C), red (O).

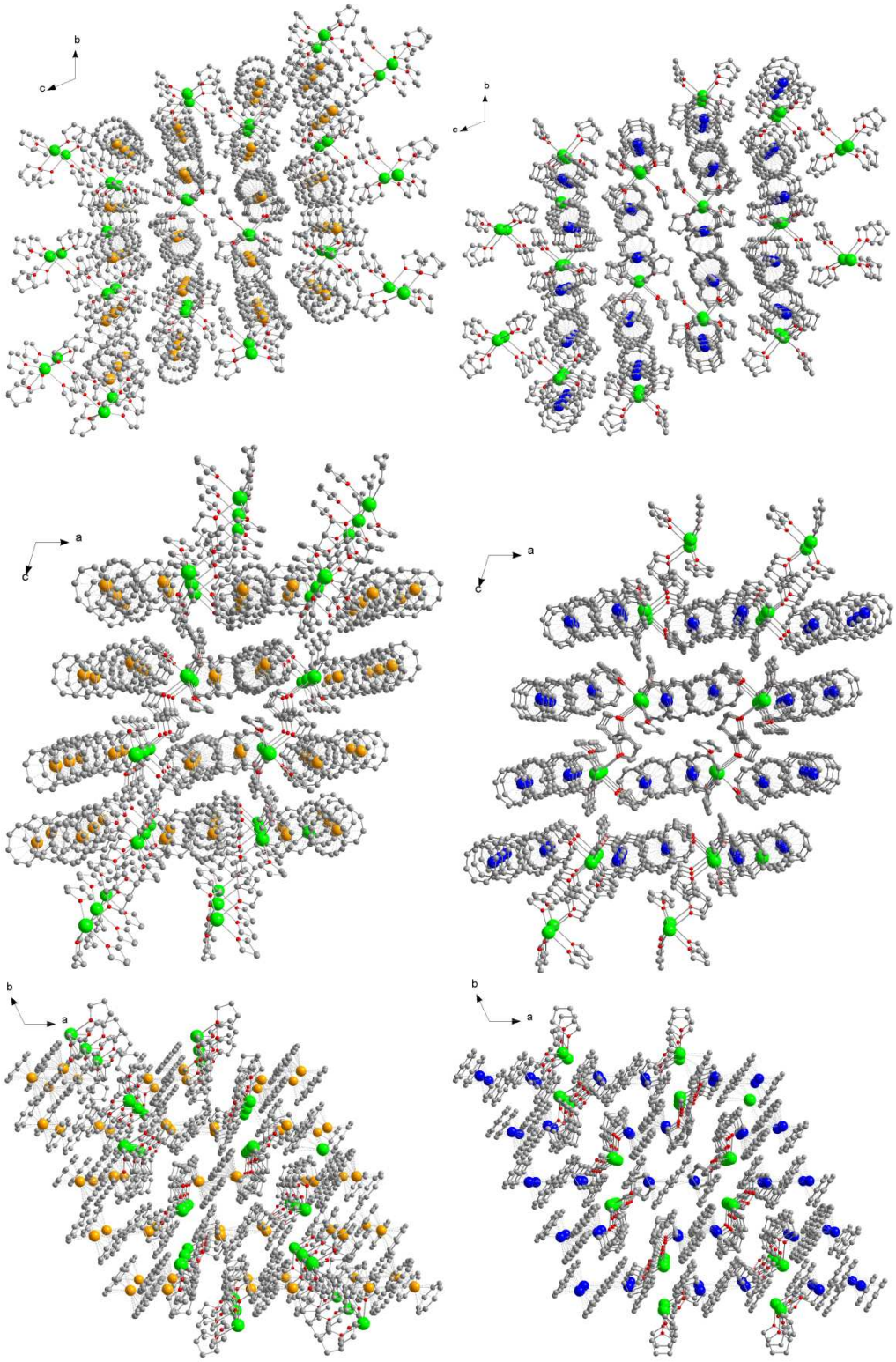

Figure S4. Packing arrangement of **2** (left) and **3** (right) looking down the *a* (top) *b* (center) and *c* (bottom) axis. H atoms are omitted for clarity. Colour code: Blue (Er^{III}), Orange (Gd^{III}), light green (K), grey (C), red (O).

Table S1. Selected Crystallographic data for **1-3**.

	1	2	3
CCDC	974992	974993	974994
Nearest M^{III}-M^{III} intermolecular distance (Å)	9.1947(6)	7.1256(4)	7.1926(4)
Nearest M^{III}-M^{III} intramolecular distance (Å)	4.1109(5)	8.9282(5)	8.8189(5)
M_r (g/mol)	1080.06	1097.69	1117.710
Formula	$C_{42}H_{72}Er_2Si_6$	$C_{48}H_{64}Gd_2K_2O_4$	$C_{48}H_{64}Er_2K_2O_4$
T(K)	200(2)	200(2)	200(2)
γ (Å)	0.71073	0.71073	0.71073
Crystal system	tetragonal	triclinic	triclinic
Space group	*I-4*	*P -1*	*P -1*
***a* (Å)**	16.8620(4)	12.5506(3)	12.4865(10)
***b* (Å)**	16.8620(4)	12.9933(3)	12.8999(10)
***c* (Å)**	20.2149(5)	16.7384(4)	16.7853(15)
α (deg)	90	107.0633(13)	107.250(2)
β (deg)	90	98.5557(14)	98.705(2)
γ (deg)	90	112.1212(13)	111.302(2)
V ($Å^3$)	5747.6(3)	2311.45(10)	2301.4(3)
ρ_{calc} (cm^{-3})	1.248	1.577	1.613
Z	8	2	2
Reflections collected	28967	13089	19618
Goodness of fit	1.012	1.034	1.046
R1	0.0277	0.0409	0.0837
wR2	0.0630	0.0826	0.1559
Reflections with *I* □2σ(*I*)	6433	9370	7065

2. Magnetic data

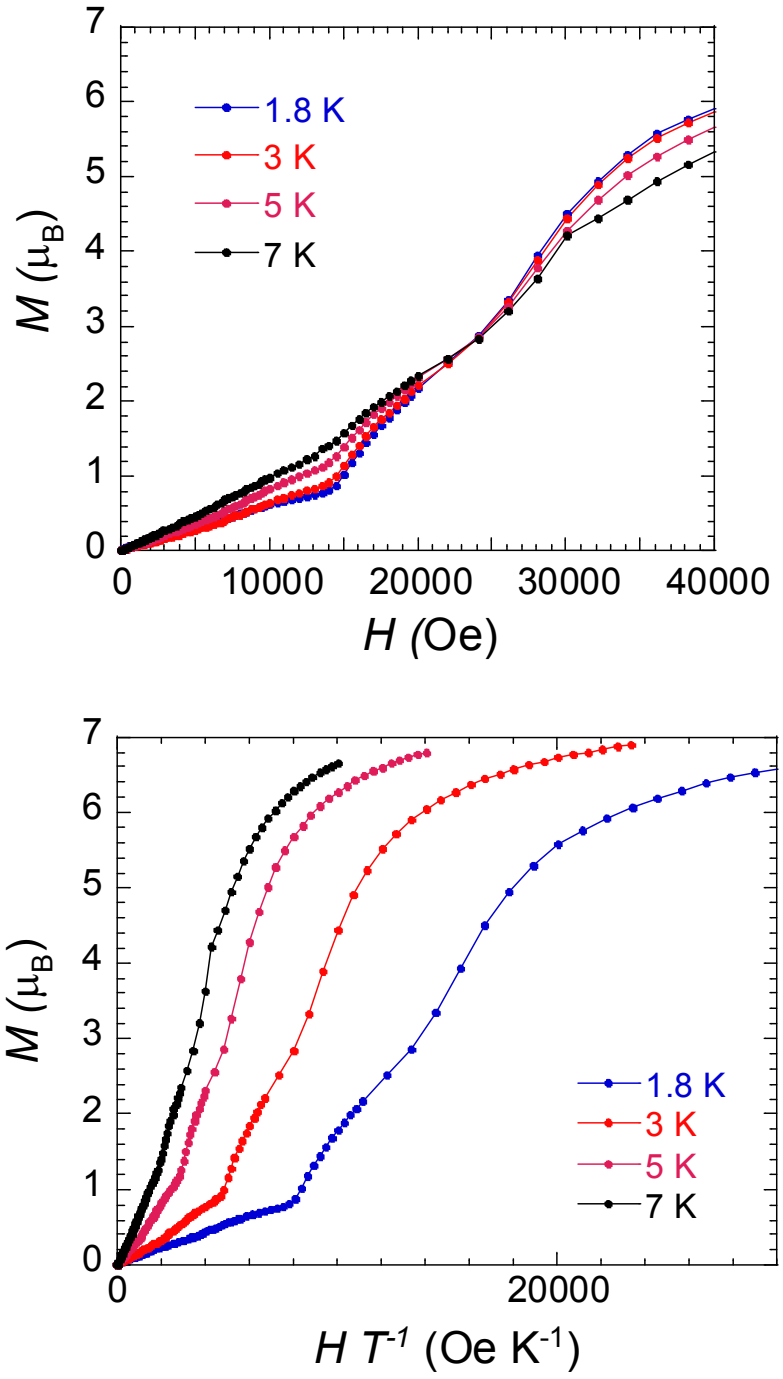

Figure S5. Solid state field dependence of the magnetization (top) and reduced magnetization (bottom) for **1** at the indicated temperatures.

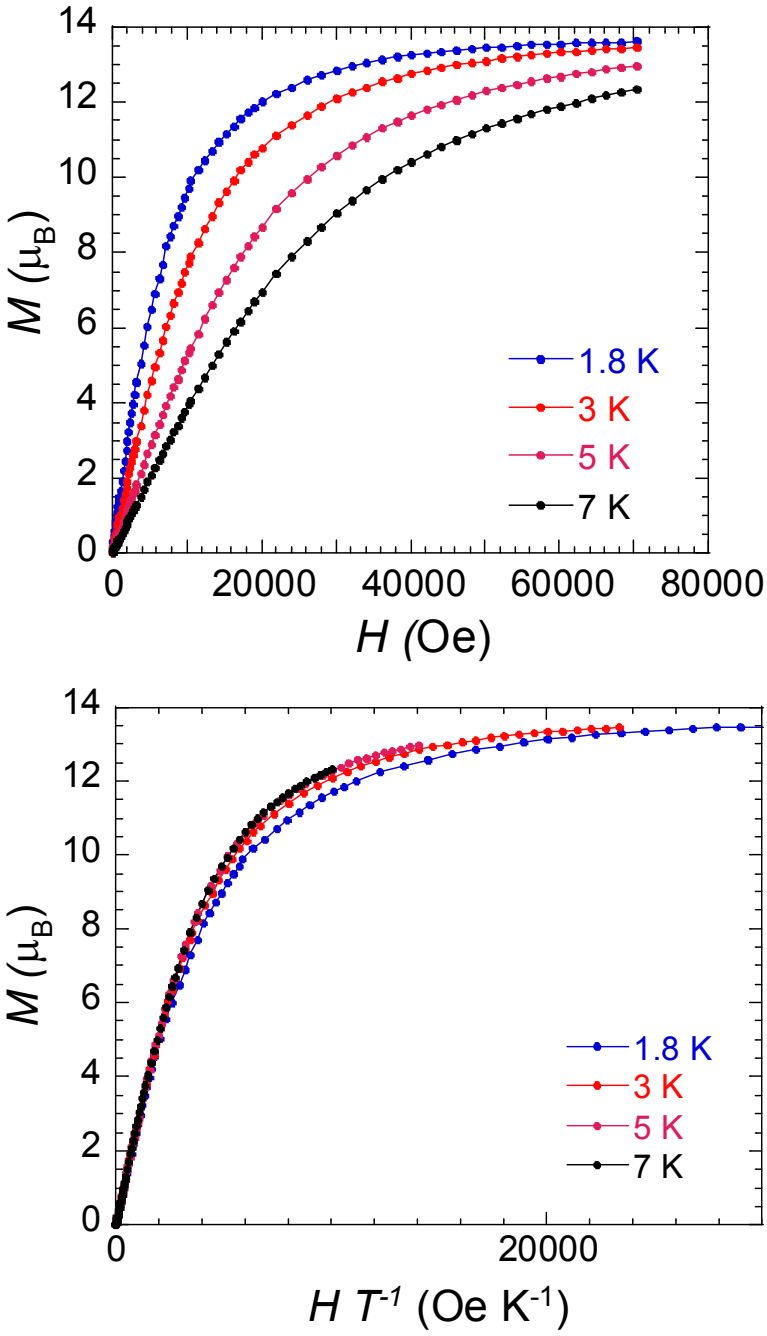

Figure S6. Solid state field dependence of the magnetization (top) and reduced magnetization (bottom) for **2** at the indicated temperatures.

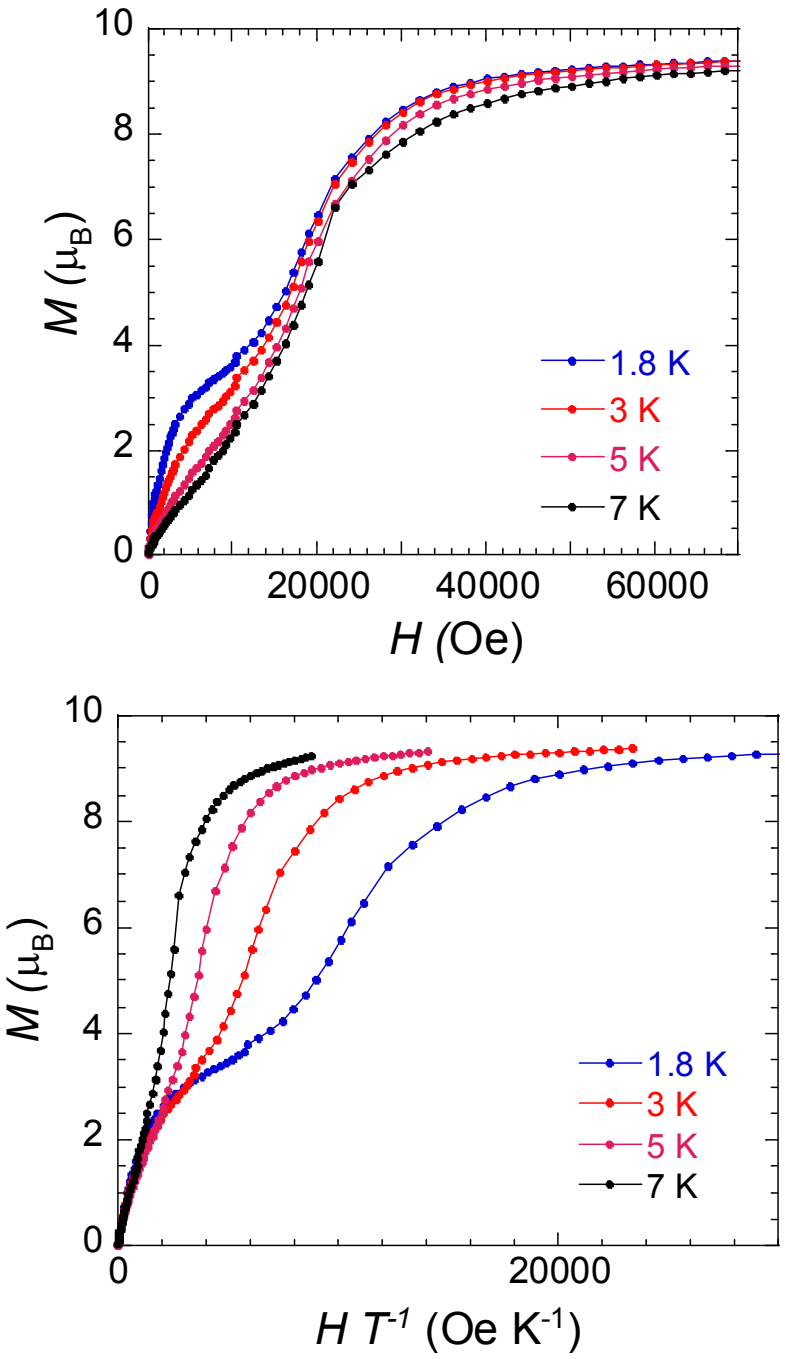

Figure S7. Solid state field dependence of the magnetization (top) and reduced magnetization (bottom) for **3** at the indicated temperatures.

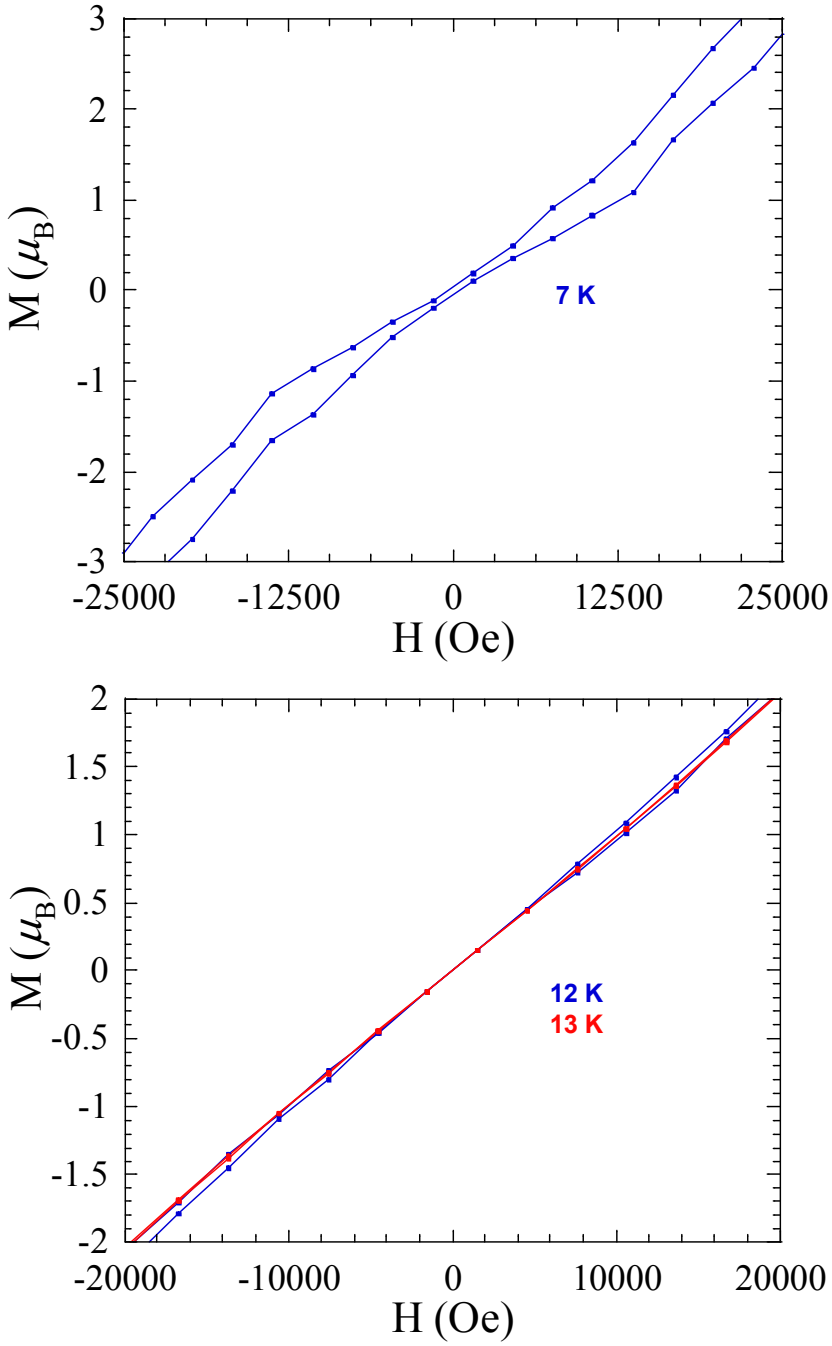

Figure S8. Solid state magnetic hysteresis data for **1** at indicated temperatures using an average sweep rate of 22 Oe.s^{-1}. Solid lines are guides for the eye. Coercivity is observed up to 7 K at *M*=0 (Top). Openings in the hysteresis are observed up to 12 K at M≠0 (bottom).

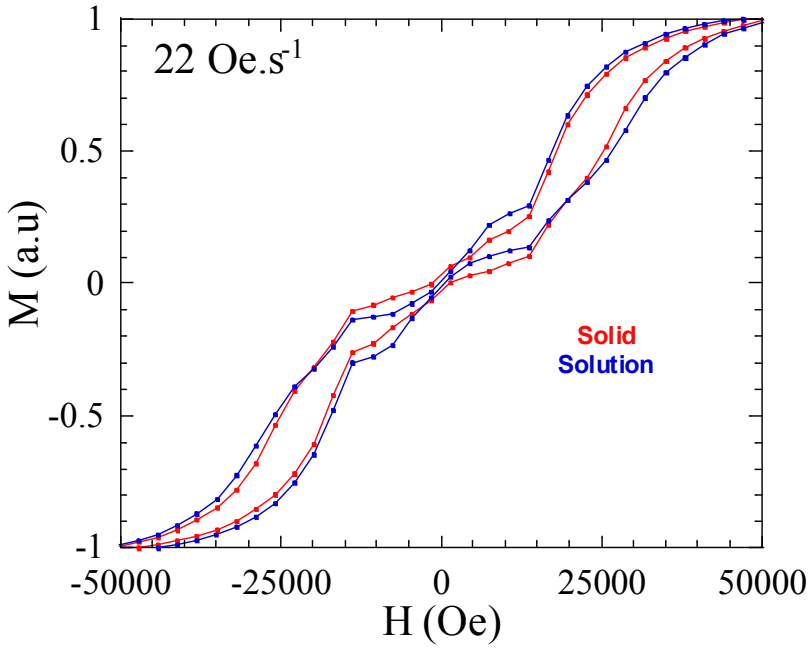

Figure S9. Solid state magnetic hysteresis data for **1** (●) and a 4 mM cyclopentane solution of **1** (●) at 1.8 K using an average sweep rate of 22 Oe.s^{-1}. Solid lines are guides for the eye.

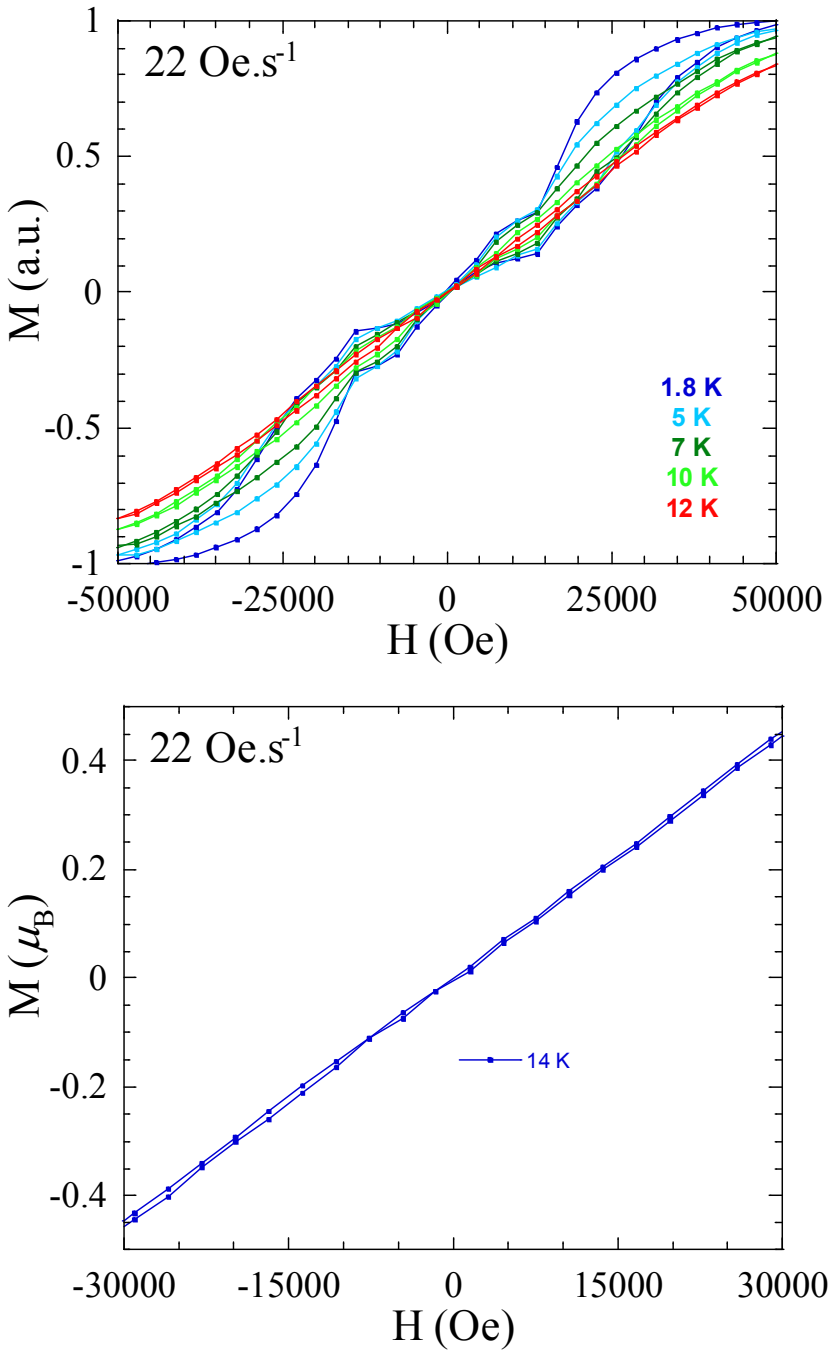

Figure S10. Normalized magnetic hysteresis data of a 4 mM Cyclopentane solution of **1** over the indicated temperature range (top), and at 14 K (bottom). In all measurements the average sweep rate is 22 Oe.s^{-1}. Solid lines are guides for the eye.

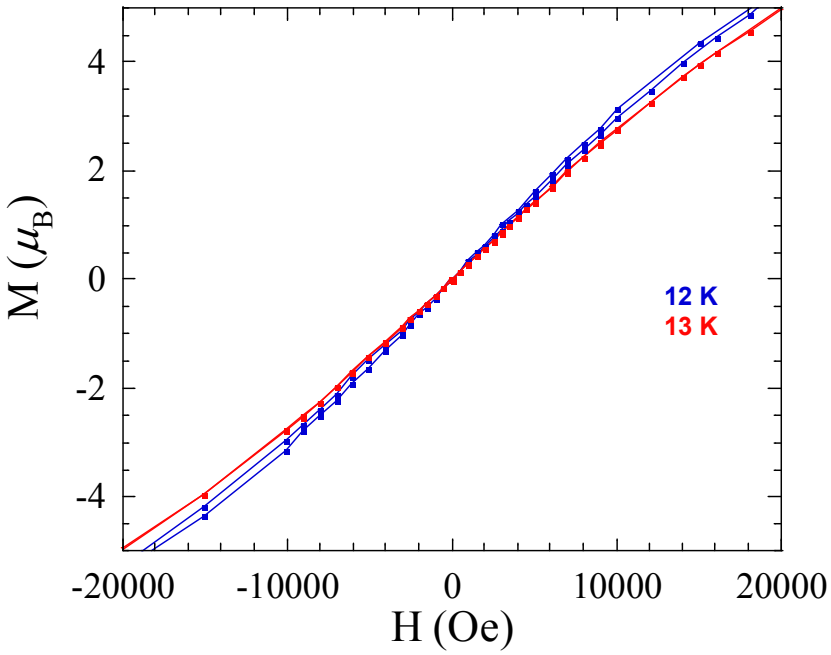

Figure S11. Solid-state magnetic hysteresis data for **3** at 12 K and 13 K using an average sweep rate of 22 Oe.s^{-1}. Solid lines are guides for the eye.

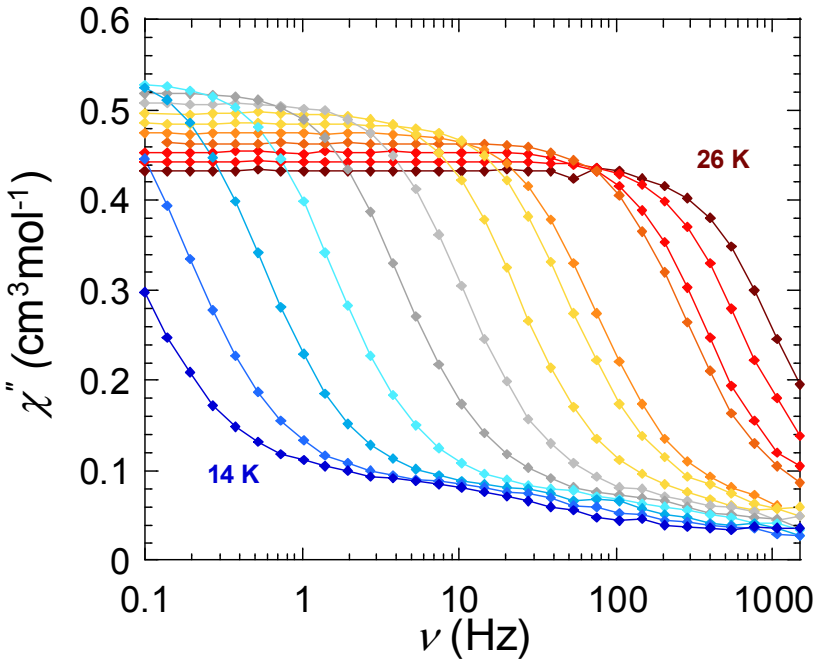

Figure S12. Solid state variable temperature in-phase (χ') magnetic susceptibility of **1** under 0 Oe dc field and the indicated temperature range.

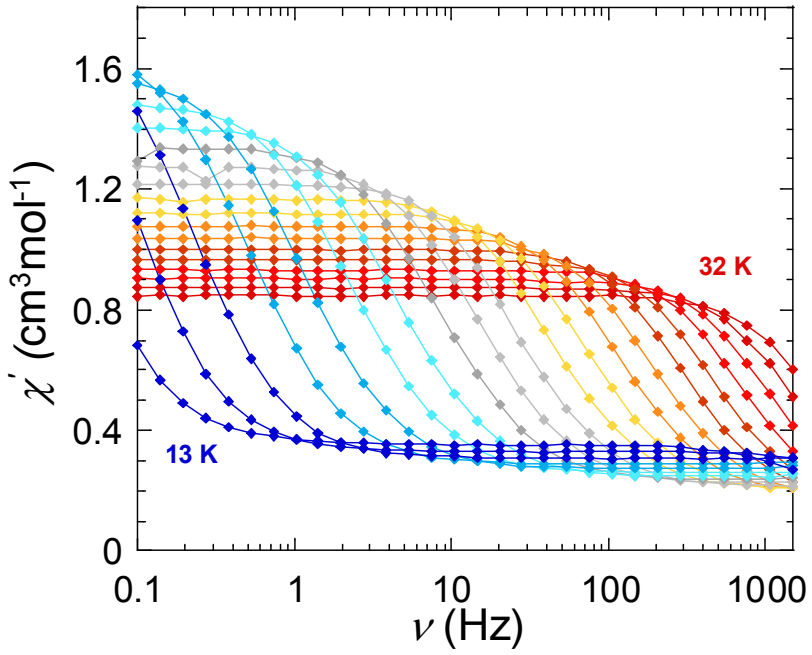

Figure S13. Solid state variable temperature in-phase (χ') magnetic susceptibility of **3** under 0 Oe dc field and the indicated temperature range.

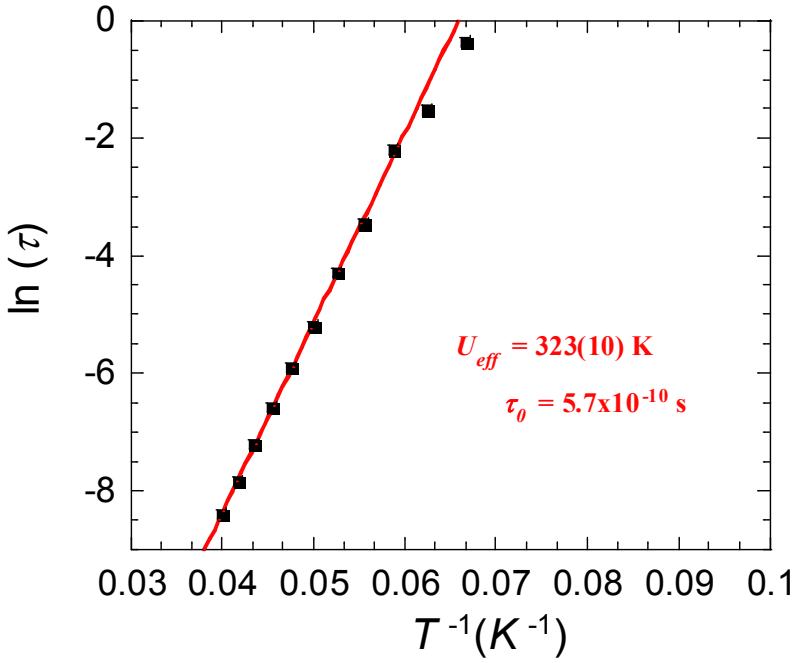

Figure S14. Solid-state relaxation time of the magnetization ln(τ) *vs*. T^{-1} for **1** (Arrhenius plot using ac data) under 0 Oe applied field. The solid line corresponds to the fit.

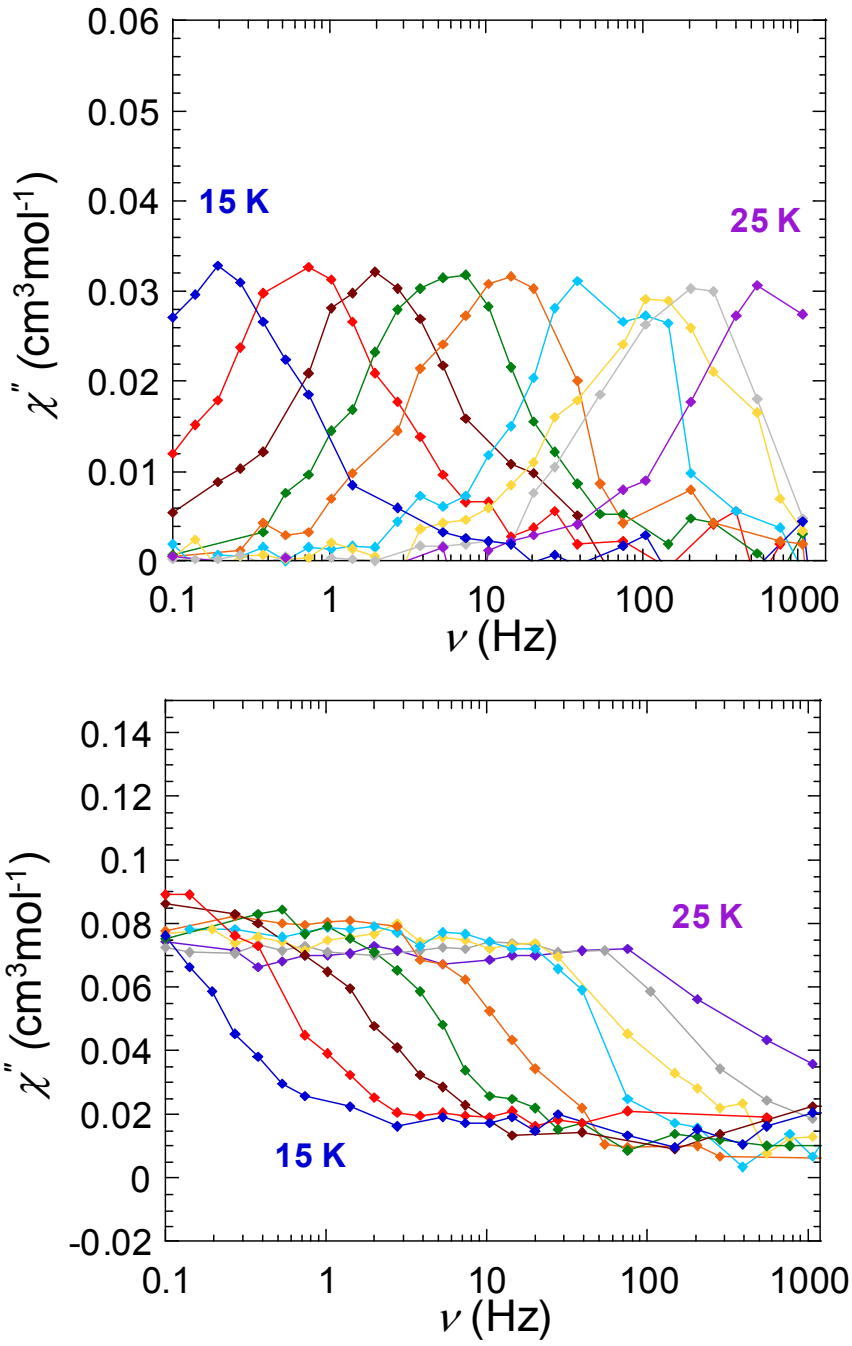

Figure S15. Variable temperature in-phase (top) and out-of phase (bottom) magnetic susceptibility of a 4 mM cyclopentane solution of **1** under 0 Oe dc field and the indicated temperature range.

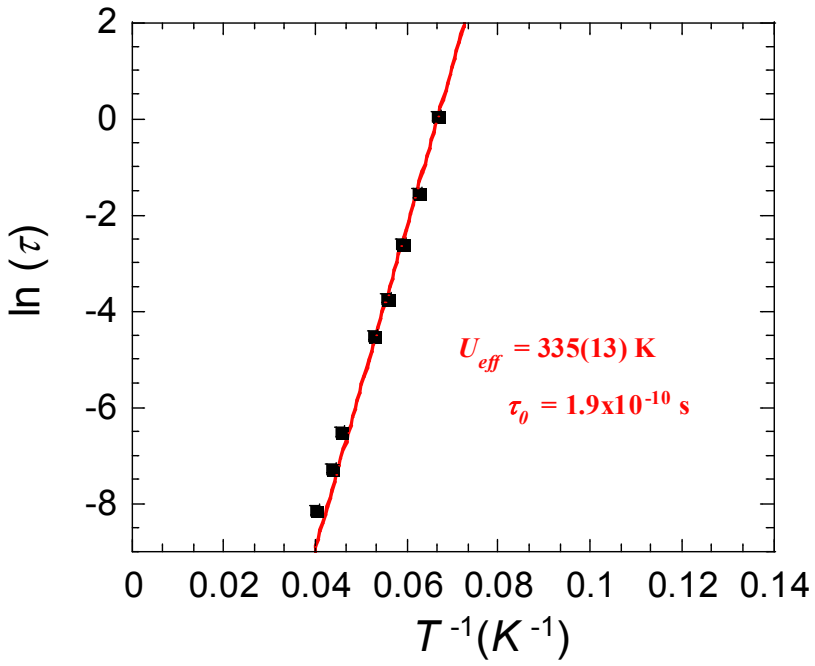

Figure S16. Relaxation time of the magnetization ln(τ) *vs*. T^{-1} for 4 mM cyclopentane solution of **1** (Arrhenius plot using ac data) under 0 Oe applied field. The solid line corresponds to the fit.

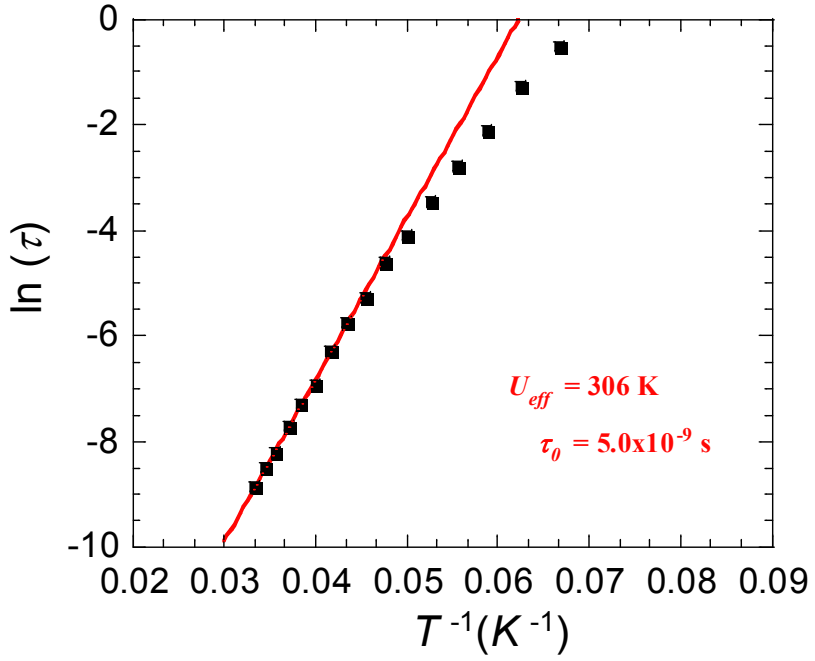

Figure S17. Solid-state relaxation time of the magnetization ln(τ) *vs*. T^{-1} for **3** (Arrhenius plot using ac data) under 0 Oe applied field. The solid line corresponds to the fit.

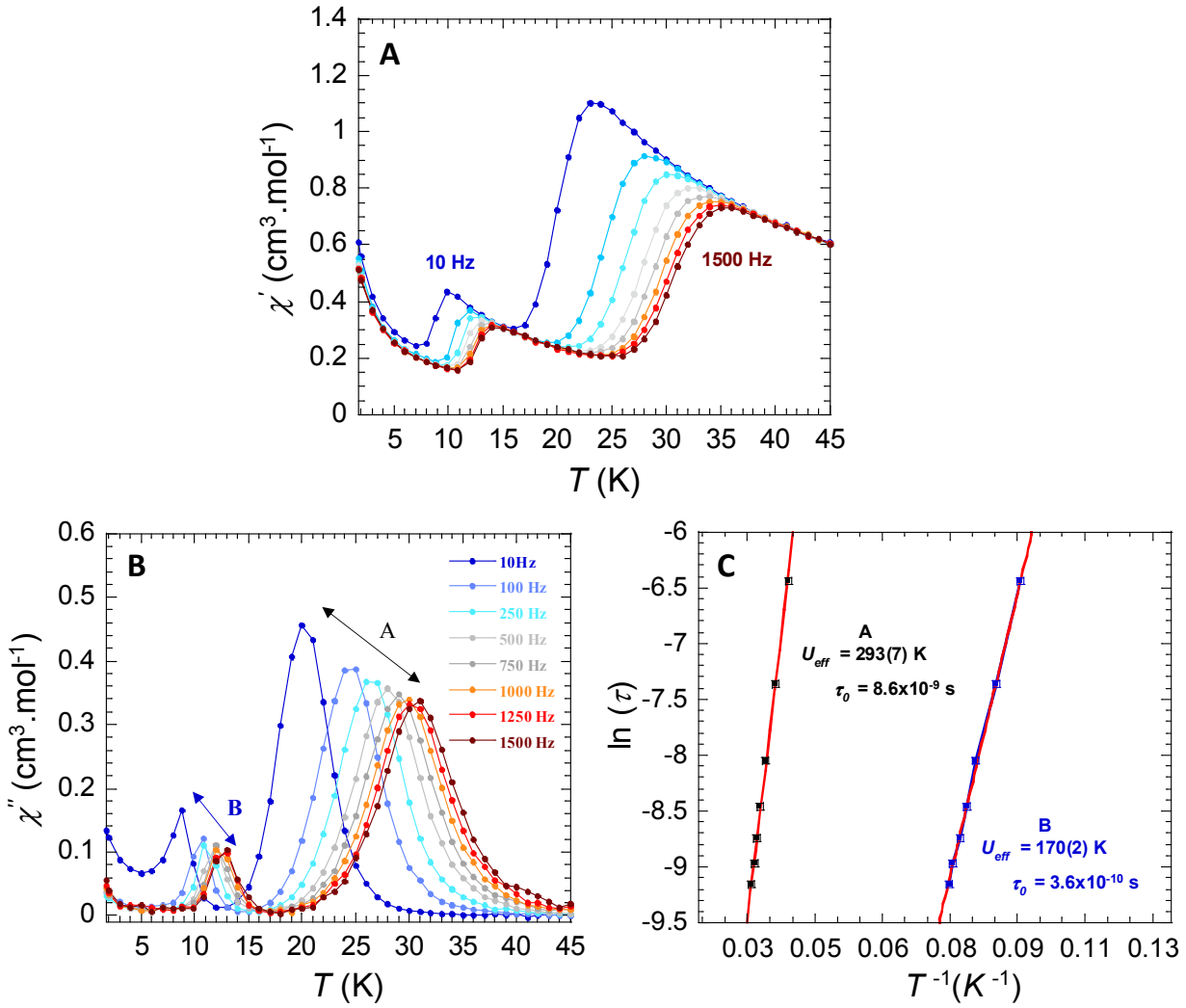

Figure S18. Temperature dependence of in-phase χ' (A) and out-of-phase χ'' (B) ac susceptibility signals under 0 Oe dc field for **3** over the indicated frequency range. (C) Relaxation time of the magnetization ln(τ) *vs*. T^{-1} for **3** (Arrhenius plot using ac data) under 0 Oe applied field. Data extracted for fit A and B corresponds to the respective peak maxima in plot B. The solid lines corresponds to the fit of the data.

3. Ab initio calculations

Table S2. Contractions of the employed basis sets for all atoms.

Basis 1	**Basis 2**
Dy.ANO-RCC...7s6p4d3f1g.	Dy.ANO-RCC...8s7p5d4f2g1h.
Lu.ANO-RCC...7s6p4d3f1g.	Lu.ANO-RCC...7s6p4d3f1g.
Cl.ANO-RCC...4s3p1d. (close)	Cl.ANO-RCC...5s4p2d1f. (close)
Cl.ANO-RCC...4s3p. (distant)	Cl.ANO-RCC...3s2p. (distant)
O.ANO-RCC...3s2p1d. (close)	O.ANO-RCC...4s3p2d1f. (close)
O.ANO-RCC...3s2p. (distant)	O.ANO-RCC...2s1p. (distant)
N.ANO-RCC...3s2p1d. (close)	N.ANO-RCC...4s3p2d1f. (close)
N.ANO-RCC...3s2p. (distant)	N.ANO-RCC...2s1p. (distant)
C.ANO-RCC...3s2p.	C.ANO-RCC...3s2p. (close)
H.ANO-RCC...2s.	C.ANO-RCC...2s1p. (distant)
	H.ANO-RCC...1s.

3.1. Fragment CASSCF/RASSI/SINGLE_ANISO calculations on individual Er^{III} ions in $Er^{III}_2COT"_3$ (1)

Table S3. Energy of the lowest spin-orbit Kramers doublets (cm^{-1}).

Basis 1	**Basis 2**
0.0	**0.0**
173.5	**167.8**
266.6	**230.6**
330.4	295.7
379.1	365.7
425.2	393.7
489.7	466.2
509.4	484.9
6604.4	6603.6
6809.8	6802.2
6876.0	6843.1
6914.7	6883.4
6944.9	6929.8
6969.8	6942.8
7002.8	6980.5
10703.4	10697.3
10872.6	10859.5
...	...

Table S4. *g* tensors of the low-lying Kramers doublets (KD).

KD		Basis 1	Basis 2
1	g_X	3.5×10^{-6}	4.6×10^{-6}
	g_Y	4.9×10^{-6}	6.4×10^{-6}
	g_Z	17.95770	17.95758
2	g_X	0.00112	0.00217
	g_Y	0.00122	0.00244
	g_Z	15.53793	15.53596
3	g_X	11.27460	11.11520
	g_Y	7.87820	8.04546
	g_Z	1.18534	1.19239
4	g_X	1.57036	1.41329
	g_Y	1.80976	1.64757
	g_Z	3.62725	3.62391
5	g_X	0.00035	0.00097
	g_Y	0.00581	0.00463
	g_Z	13.09161	13.09230
6	g_X	0.33121	0.30915
	g_Y	0.54587	0.51303
	g_Z	6.07004	6.07357
7	g_X	0.22024	0.21487
	g_Y	0.35282	0.37802
	g_Z	12.31155	12.02050
8	g_X	0.08459	0.03188
	g_Y	0.14514	0.07287
	g_Z	13.80698	14.04325

Table S5. Angles between the main magnetic axes of the lowest Kramers doublet obtained in different computational approximations (degrees).

	Basis 1	Basis 2
Basis 1	0.0000	0.0295
Basis 2	0.0295	0.0000

Table S6. Angles between the main magnetic axes of the lowest and first excited Kramers doublets obtained in different computational approximations (degrees).

Basis 1	Basis 2
0.230	0.287

Table S7. Angle between the main magnetic axis of the lowest Kramers doublet and the Er1-Er2 direction (degrees).

Basis 1	Basis 2
2.505	2.478

Table S8. Angle between the main magnetic axis of the lowest Kramers doublet of both centers Er1 and Er1'' in both computational approximations (degrees).

Basis 1	Basis 2
4.260	4.201

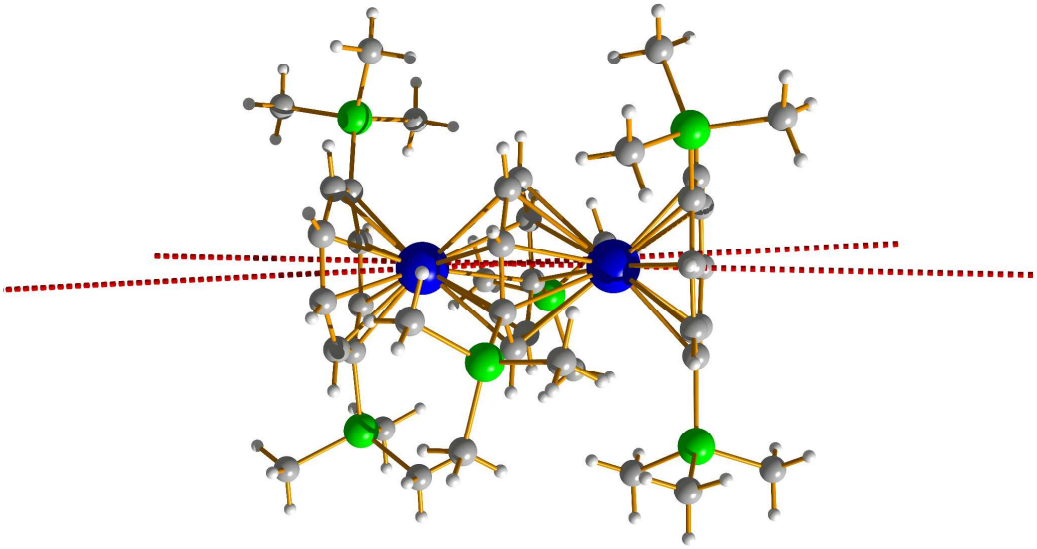

Figure S19. Orientation of the main anisotropy axes of both Er^{III} ions in $[Er_2COT"]_3$, **(1)**.

3.2. Fragment CASSCF/RASSI/SINGLE_ANISO calculations on $(C_8H_8)_4Er^{III}_2K_2(THF)_4$ (3)

Table S9. Energy of the lowest spin-orbit Kramers doublets (cm^{-1}).

conformer 1				conformer 2			
Er1		Er2		Er1		Er2	
Basis 1	Basis 2	Basis 1	Basis 2	Basis 1	Basis 2	Basis 1	Basis 2
0.0	**0.0**	**0.0**	**0.0**	**0.0**	**0.0**	**0.0**	**0.0**
188.5	**181.0**	**187.0**	**178.9**	**188.6**	**181.0**	**186.4**	**178.1**
235.9	**189.8**	**245.0**	**197.9**	**235.9**	**189.8**	**244.4**	**197.9**
315.0	270.5	321.4	275.4	315.0	270.5	320.8	275.4
420.0	395.3	414.0	393.0	420.0	395.3	415.2	394.6
437.1	402.2	438.3	396.0	437.1	402.2	438.8	396.3
537.0	501.1	533.8	495.4	537.0	501.1	534.1	496.2
545.6	517.2	539.6	508.8	545.6	517.2	540.4	509.5
6608.4	6607.7	6608.3	6607.2	6608.4	6607.7	6608.2	6607.1
6835.1	6816.7	6832.6	6820.1	6835.1	6816.8	6832.1	6818.6
6861.2	6826.7	6867.4	6824.7	6861.2	6826.7	6867.0	6825.4
6910.1	6869.7	6914.5	6872.3	6910.1	6869.7	6915.1	6873.4
6978.1	6947.4	6975.4	6946.0	6978.0	6947.5	6974.7	6945.4
6988.4	6963.2	6988.2	6957.8	6988.4	6963.2	6989.5	6959.2
7031.9	7002.7	7029.3	6997.9	7031.8	7002.7	7029.7	6998.4
10713.9	10706.5	10713.3	10705.2	10713.8	10706.5	10713.3	10705.1
10898.3	10869.7	10896.7	10873.2	10898.2	10869.7	10896.1	10871.4
...	...	...	...	...	...	...	...

Table S10. *g* tensors of the low-lying Kramers doublets (KD).

KD		conformer 1				conformer 2			
		Er1		Er2		Er1		Er2	
		Basis 1	Basis 2	Basis 1	Basis 2	Basis 1	Basis 2	Basis 1	Basis 2
	g_X	0.00004	0.00005	0.00000	0.00000	0.00004	0.00005	0.00011	0.00013
1	g_Y	0.00004	0.00005	0.00000	0.00000	0.00004	0.00005	0.00013	0.00016
	g_Z	17.94304	17.94271	17.94407	17.94433	17.94301	17.94271	17.93748	17.93739
	g_X	0.00657	0.04704	0.00480	0.02693	0.00669	0.04674	0.01455	0.06896
2	g_Y	0.00746	0.06979	0.00507	0.03108	0.00760	0.06945	0.01607	0.08564
	g_Z	15.47205	15.33312	15.51483	15.47665	15.47191	15.33211	15.46999	15.38611
	g_X	10.27611	10.08143	10.52866	10.42901	10.27687	10.08169	10.80332	10.64982
3	g_Y	8.80954	8.87881	8.59012	8.65488	8.80881	8.87700	8.27911	8.36930
	g_Z	1.23738	1.28267	1.21964	1.24143	1.23738	1.28354	1.22790	1.25945
	g_X	0.41604	0.36930	0.78748	0.72882	0.41724	0.37077	0.79602	0.73838
4	g_Y	1.06649	0.98982	1.15246	1.07147	1.06687	0.99085	1.71656	1.60897
	g_Z	3.74856	3.76686	3.66207	3.66874	3.74853	3.76676	3.77766	3.76185
	g_X	0.00787	0.13670	0.00786	0.07324	0.00802	0.13576	0.01316	0.01534
5	g_Y	0.03125	0.44601	0.01286	0.21697	0.03150	0.44662	0.07289	0.64136
	g_Z	12.98068	6.29528	13.05396	10.14998	12.98078	6.29365	12.95306	10.36982
	g_X	0.14273	0.00804	0.19304	0.09592	0.14522	0.00792	0.00196	0.04457
6	g_Y	0.51266	0.04288	0.55539	0.31570	0.50915	0.04275	1.00701	0.43555
	g_Z	6.10661	12.83605	6.07579	9.08096	6.10665	12.83749	6.06727	8.58098
7	g_X	0.00626	0.08006	0.34491	0.07886	0.00574	0.08104	0.14983	0.21023

	g_Y	0.32272	0.25477	0.77590	0.56277	0.31847	0.25539	0.83402	0.66259
	g_Z	9.35382	8.66847	9.24615	8.57329	9.34659	8.66804	9.67792	8.65764
	g_X	0.15135	0.06425	0.49670	0.21281	0.14889	0.06402	0.43815	0.19709
8	g_Y	0.21104	0.12086	0.72387	0.27965	0.20842	0.12046	0.61640	0.24487
	g_Z	11.41606	10.95462	11.27301	10.89218	11.41051	10.95390	11.57244	10.95418

Table S11. Angles between the main magnetic axes of the lowest Kramers doublet obtained in different computational approximations of both magnetic centers of the **conformer 1** (degrees)..

		Er1 conformer 1		Er2 conformer 1	
		Basis 1	**Basis 2**	**Basis 1**	**Basis 2**
Er1 conformer 1	**Basis 1**	0.000	0.007	10.615	10.605
	Basis 2	0.007	0.000	10.613	10.602
Er2 conformer 1	**Basis 1**	10.615	10.613	0.000	0.020
	Basis 2	10.605	10.602	0.020	0.000

Table S12. Angles between the main magnetic axes of the lowest Kramers doublet obtained in different computational approximations of both magnetic centers of the **conformer 2** (degrees).

		Er1 conformer 2		Er2 conformer 2	
		Basis 1	**Basis 2**	**Basis 1**	**Basis 2**
Er1 conformer 2	**Basis 1**	0.000	0.009	10.229	10.220
	Basis 2	0.009	0.000	10.224	10.214
Er2 conformer 2	**Basis 1**	10.229	10.224	0.000	0.013
	Basis 2	10.220	10.214	0.013	0.000

Table S13. Angles between the main magnetic axes of the lowest and first excited Kramers doublets obtained in different computational approximations (degrees).

conformer 1				**conformer 2**			
Er1		**Er2**		**Er1**		**Er2**	
Basis 1	**Basis 2**	**Basis 1**	**Basis 2**	**Basis 1**	**Basis 2**	**Basis 1**	**Basis 2**
0.6657	1.3297	0.7303	0.7992	0.6680	1.3343	0.2749	0.1154

Table S14. Angle between the main magnetic axis of the lowest Kramers doublet and the Er1-Er2 direction (degrees).

conformer 1				**conformer 2**			
Er1		**Er2**		**Er1**		**Er2**	
Basis 1	**Basis 2**	**Basis 1**	**Basis 2**	**Basis 1**	**Basis 2**	**Basis 1**	**Basis 2**
4.6770	4.6757	6.0842	6.0713	4.6777	4.6747	5.8214	5.8105

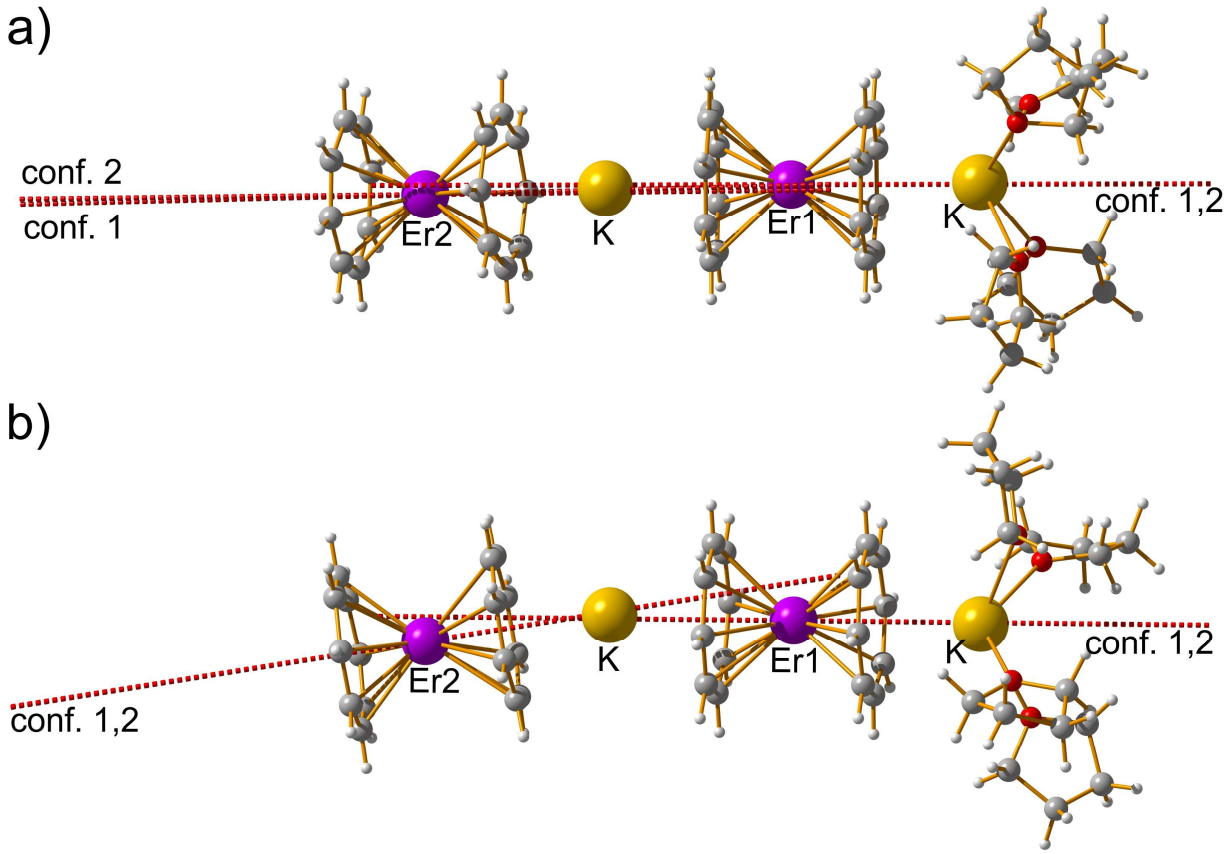

Figure S20. Two views of the orientations of local magnetic axes on both Er^{III} ions in both conformers of the $[(COT)_4Er^{III}_2K_2(THF)_4]$, **(3)** basis 2.

3.3. Analysis of the multiplet-specific crystal-field for individual Er ions in $Er^{III}_2COT"_3$ (1) and $(C_8H_8)_4Er^{III}_2K_2(THF)_4$ (3) from *ab initio* calculations

Recently, the extraction of the parameters of the multiplet-specific crystal-field for lanthanides methodology has been implemented in the SINGLE_ANISO program in MOLCAS. The results presented below use the ab initio CASSCF/RASSI wave function and energies to compute the parameters of the crystal-field splitting of the ground *J* multiplet.

The Crystal-Field Hamiltonian:

$$H_{CF} = \sum_{k,q} B_k^q O_k^q$$

where:

O_k^q -- Extended Stevens Operators (ESO)as defined in:

1. Rudowicz, C.; *J. Phys. C*: *Solid State Phys*., **1985**, *18*, 1415-1430.
2. Implemented in the "EasySpin" function in MATLAB, www.easyspin.org.

k - the rank of the ITO, = 2, 4, 6.

q - the component (projection) of the ITO, = *-k*, *-k+1*, ... *0*, *1*, ...*k*;

v

Quantization axis was chosen the main magnetic axis of the ground Kramers doublet.

Table S15. Parameters of the Crystal-Field acting on the ground atomic multiplet *J*=15/2 for individual Er ions in $\mathbf{Er^{III}_2COT"_3}$ (1).

k	q	basis 1	basis 2
	-2	0.1887090E+00	0.1800500E+00
	-1	0.3161768E+00	0.2554204E+00
2	0	**-0.1893583E+01**	**-0.1669436E+01**
	1	0.2587158E+00	0.3140670E+00
	2	-0.5246091E-01	0.9268839E-02
	-4	-0.1633209E-03	-0.3442503E-03
	-3	-0.8098237E-03	-0.8476980E-03
	-2	0.5815029E-03	0.6062681E-03
	-1	-0.1232699E-02	-0.6171347E-03
4	0	**-0.1041120E-01**	**-0.1052946E-01**
	1	-0.2771811E-02	-0.2926116E-02
	2	-0.1225984E-03	0.5536521E-04
	3	-0.3266207E-03	-0.9131847E-03
	4	0.3375601E-03	0.1377940E-03
	-6	0.1282839E-04	0.1479890E-04
	-5	-0.2215943E-04	-0.6724200E-04
	-4	-0.8339451E-05	-0.1176817E-04
6	-3	-0.5974531E-04	-0.4939148E-04
	-2	0.1570049E-05	0.6079867E-05
	-1	-0.7652788E-05	-0.1229260E-04

0	0.5310402E-04	0.5262059E-04
1	0.2040769E-04	0.1793330E-04
2	-0.1313619E-04	-0.1141820E-04
3	-0.2018481E-05	-0.3405120E-04
4	0.8190713E-05	0.1189309E-06
5	0.7197491E-04	0.3054089E-04
6	-0.9950552E-05	0.6701115E-05

Table S16. Parameters of the Crystal-Field acting on the ground atomic multiplet *J*=15/2 for individual Er ions in **$(C_8H_8)_4Er^{III}_2K_2(THF)_4$ (3)** (Basis 2).

k	q	conformer 1		conformer 2	
		Er1	Er2	Er1	Er2
	-2	0.1534402E+00	-0.4692461E-01	0.1532079E+00	-0.2212196E+00
	-1	0.3266770E-01	-0.8153065E-01	0.3412220E-01	0.1050928E+00
2	**0**	**-0.1475391E+01**	**-0.1513222E+01**	**-0.1475472E+01**	**-0.1515696E+01**
	1	0.9200708E-01	-0.3089926E-01	0.9095677E-01	0.4746250E-01
	2	0.4394529E-01	0.1567050E+00	0.4491013E-01	-0.5158360E-02
	-4	0.2029819E-02	0.7459578E-03	0.2028673E-02	0.3749667E-04
	-3	0.1996333E-02	-0.1416839E-02	0.1996214E-02	-0.1389115E-02
	-2	0.2813802E-03	-0.4474899E-04	0.2809513E-03	-0.5100006E-03
	-1	-0.1294201E-05	0.1429163E-03	-0.1888793E-04	0.2175580E-03
4	**0**	**-0.1272882E-01**	**-0.1229198E-01**	**-0.1272897E-01**	**-0.1229424E-01**
	1	0.2249410E-03	-0.1527666E-02	0.2406330E-03	-0.1073093E-02
	2	-0.9599341E-04	0.3224323E-03	-0.9397602E-04	0.1339960E-03
	3	-0.8660395E-03	0.1986894E-02	-0.8612216E-03	-0.1611504E-03
	4	0.4522761E-03	0.4043828E-03	0.4545887E-03	0.2271430E-02
	-6	-0.9088685E-05	0.1672247E-04	-0.9111312E-05	-0.1522397E-04
	-5	0.7084730E-05	0.3921679E-04	0.6910743E-05	0.2095764E-03
	-4	0.5629869E-04	0.2225964E-04	0.5627614E-04	0.1990306E-05
	-3	0.6736473E-04	-0.4756768E-04	0.6737688E-04	-0.3174834E-04
	-2	-0.1498977E-04	0.6391606E-05	-0.1494835E-04	0.9217882E-05
	-1	-0.6375505E-05	0.6401946E-05	-0.6227237E-05	-0.1402378E-04
6	**0**	0.6286700E-04	0.6079353E-04	0.6286673E-04	0.6089208E-04
	1	-0.1300096E-04	0.3061934E-04	-0.1316884E-04	0.1385296E-04
	2	-0.3598898E-05	-0.6797838E-05	-0.3693327E-05	0.3032052E-05
	3	-0.9770542E-05	0.4987824E-04	-0.9674421E-05	0.3097636E-05
	4	0.1449333E-04	0.1171686E-04	0.1456096E-04	0.6617635E-04
	5	0.2762864E-03	-0.1484112E-03	0.2762005E-03	0.1585460E-03
	6	-0.1821765E-05	-0.8866015E-05	-0.1822213E-05	-0.1886963E-04

3.4. Intramolecular magnetic interactions in $Er^{III}_2COT"_3$ (1) and $(C_8H_8)_4Er^{III}_2K_2(THF)_4$ (3)

A) Broken Symmetry DFT calculations

Estimation of the exchange coupling was done by Broken Symmetry-DFT calculations with ORCA program package. We employed B3LYP functional, Tight Convergence energy threshold, Grid5, SVP basis sets for all atoms. Computationally, Er^{III} ions were substituted by Gd^{III} (S=7/2). The resulting exchange coupling constant corresponding to the Gd^{III}-Gd^{III} interaction was rescaled to the spins S=3/2 of Er^{III}-Er^{III} interacting ions, which corresponds to multiplication of the exchange coupling constant computed within BS-DFT for the Gd^{III}-Gd^{III} interaction by the coefficient 49/9. The obtained value corresponds to the exchange coupling constant for the Er^{III}-Er^{III} interaction within the Lines model, which describes the interaction between true spins of metal sites, in the absence of the spin-orbit coupling on metal ions. Further, the exchange interaction is written in terms of local pseudospins $\tilde{s} = 1/2$ (Ising model) of the ground Kramers Doublets of the Er^{III} ions. The relation between Lines and Ising parameters for this particular case is:

$$J_{\text{Ising}} = 9\cos\varphi \cdot J_{\text{Lines}},$$

where φ is the angle between the Z directions of the ground Kramers Doublet on each Er ions.

B) Simulations within Ising model (POLY_ANISO)

Exchange Ising Hamiltonian:

$$\hat{\mathrm{H}}_{exch} = J\hat{s}_{1,z}\hat{s}_{2,z} \qquad \textbf{(1)}$$

where $\hat{s}_{i,z}$ is the projection of the pseudospin $\tilde{s} = 1/2$ on the main magnetic axis z of the center i; J_{exch} and J_{dip} are the parameters of the total magnetic interaction between the centers (exchange and dipolar):

$$J_{total} = J_{exch} + J_{dip} \qquad \textbf{(2)}$$

The dipole-dipole interaction is taken into account exact, as all the required data is available in ab initio calculations.

$$\hat{\mathrm{H}}_{dip} = -\frac{\hat{\boldsymbol{\mu}}_1\hat{\boldsymbol{\mu}}_2 - 3\left(\hat{\boldsymbol{\mu}}_1 \cdot \mathbf{n}_{12}\right)\left(\hat{\boldsymbol{\mu}}_2 \cdot \mathbf{n}_{12}\right)}{r_{12}^3} \qquad \textbf{(3)}$$

$\hat{\mu}_1$ - matrix of the magnetic moment written in the basis of pseudospin eigenfunctions for the center *"i"*, obtained *ab initio*.

$\mathbf{n}_{12}$ – the unit vector connecting centers **1** and **2.**

Table S17. Magnetic couplings (dipolar and exchange) between Er centers (basis 2) in **$Er^{III}_2COT"_3$ (1),** with respect to the pseudospin $\tilde{s} = 1/2$ of the interacting ground Kramers doublets on Er^{III} ions (Ising parameters).

J_{dip}*	J_{exch} (BS-DFT)	$J_{total} = J_{dip}$* + J_{exch}
4.013	-36.162	-32.149

* -- contribution coming only from the Ising terms $\sim \hat{\tilde{s}}_{1,z}\hat{\tilde{s}}_{2,z}$ to the dipolar coupling.

Table S18. Magnetic couplings (dipolar and exchange) between Er centers (basis 2) in **$(C_8H_8)_4Er^{III}_2K_2(THF)_4$ (3),** with respect to the pseudospin $\tilde{s} = 1/2$ of the interacting ground Kramers doublets on Er^{III} ions.

interaction	J_{dip}*	J_{exch}(BS-DFT)	$J_{total} = J_{dip}$* + J_{exch}
conformer 1	0.40104	0.00	0.40104
conformer 2	0.40455	0.00	0.40455

* -- contribution coming only from the Ising terms $\sim \hat{\tilde{s}}_{1,z}\hat{\tilde{s}}_{2,z}$ to the dipolar coupling.

Table S19. Low-lying energy spectrum of the **$Er^{III}_2COT"_3$ (1)** (in cm^{-1}) and the g_Z values of the corresponding Ising doublets (g_X=g_Y=0).

$J=J_{exch}+J_{dip}$			$J=J_{dip}$		
energy	Δ_{tunnel}	g_Z	energy	Δ_{tunnel}	g_Z
0.00000000 0.00000000	1.10000E-10	1.2484	0.00000000 0.00000000	1.00000E-12	35.8899
15.51120586 15.51120586	3.00027E-12	35.8891	2.00704019 2.00704019	2.99982E-12	1.2661
168.01079785 168.01079785	4.85102E-09	1.2523	167.02267775 167.02267775	5.19833E-11	33.4628
168.07847657 168.07847657	1.55399E-09	1.2557	167.15781910 167.15781910	1.89857E-11	33.4628
180.07664724 180.07664724	3.80993E-10	33.4607	168.82407688 168.82407688	2.45990E-10	1.2681

182.66630225 182.66630225	3.90003E-10	33.4602	168.82746729 168.82746729	1.76982E-10	1.2685

Table S20. Low-lying energy spectrum of the **$(C_8H_8)_4Er^{III}_2K_2(THF)_4$ (3)** (in cm^{-1}) and the g_Z values of the corresponding Ising doublets (g_X=g_Y=0).

Conformer 1			Conformer 2		
energy	Δ_{tunnel}	g_Z	energy	Δ_{tunnel}	g_Z
0.00000000 0.00000000	1.70000E-13	35.7335	0.00000000 0.00000000	9.50000E-13	35.7376
0.20224856 0.20224856	3.20022E-13	3.3157	0.20218963 0.20218963	5.66999E-12	3.1941
178.92554454 178.92554454	1.35998E-10	33.2940	178.18896935 178.18896935	4.54008E-10	33.1970
179.10008020 179.10008020	1.02798E-09	3.8031	178.36240058 178.36240058	2.73300E-09	3.9177
181.04609952 181.04609952	1.95996E-10	33.1706	181.05269001 181.05269001	1.08199E-09	33.1719
181.21895944 181.21895944	1.75987E-10	3.7465	181.22550416 181.22550416	5.55301E-09	3.6590

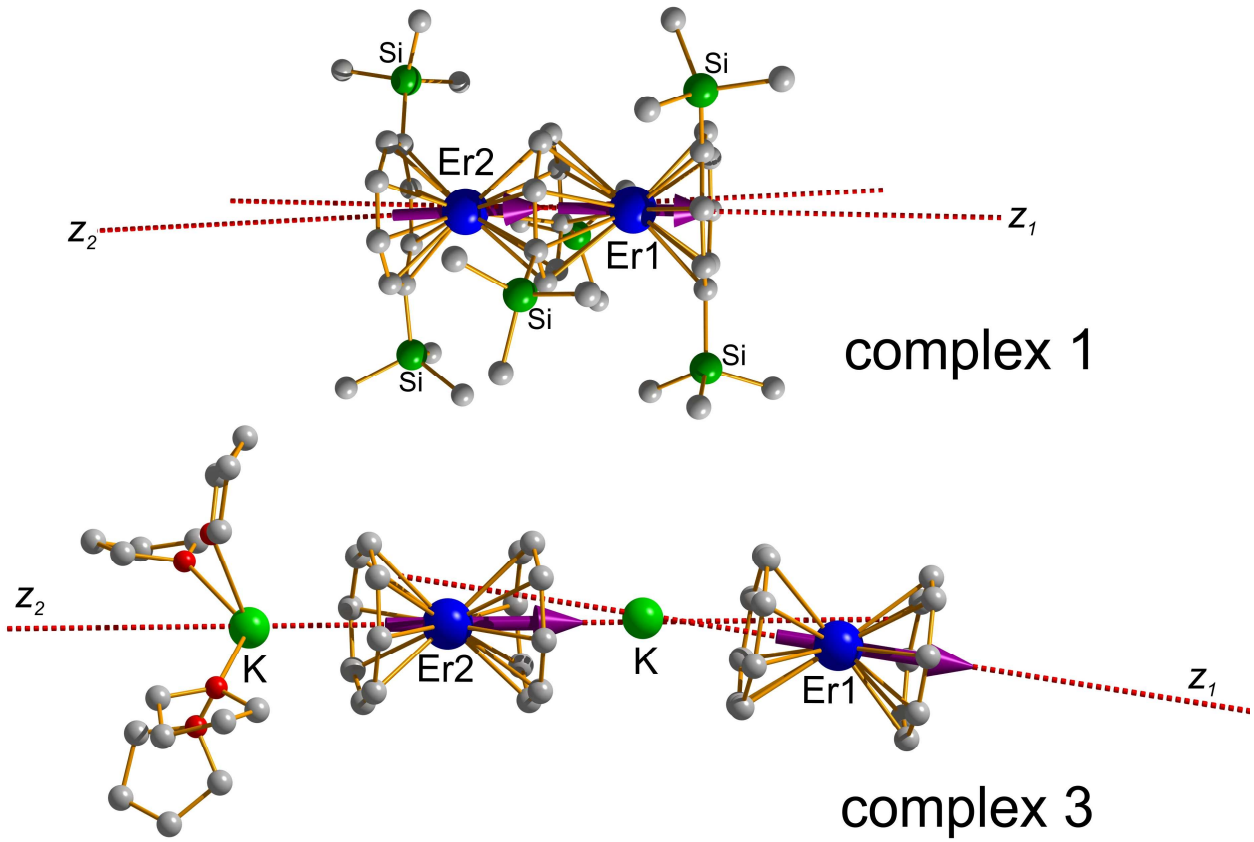

Figure S21. Orientations of local magnetic moments on both Er^{III} ions in the ground exchange doublet state of $[Er_2COT''_3]$, **(1)** (up) and $[(COT)_4Er^{III}_2K_2(THF)_4]$, **(3)** (down) when only the intramolecular dipole-dipole interaction is considered.